# Reef Carbonate Productivity During Quaternary Sea Level Oscillations

Laurent Husson, Anne-Morwenn Pastier, Kevin Pedoja, M. Elliot, D. Paillard, C. Authemayou, A.-C Sarr, Anne Schmitt, S. y Cahyarini

AGU100 ADVANCING EARTH AND SPACE SCIENCE

Geochemistry, Geophysics, Geosystems

RESEARCH ARTICLE
10.1002/2017GC007335

# Reef Carbonate Productivity During Quaternary Sea Level Oscillations

**L. Husson[1], A.-M. Pastier[2], K. Pedoja[3], M. Elliot[4], D. Paillard[5], C. Authemayou[6], A.-C. Sarr[1,5], A. Schmitt[4], and S. Y. Cahyarini[7]**

[1]ISTerre, CNRS, Université Grenoble Alpes, Grenoble, France, [2]Géosciences Rennes, CNRS, Université Rennes-1, Rennes, France, [3]M2C Caen, CNRS, Université de Caen, Caen, France, [4]LPG Nantes, CNRS, Université Nantes, Nantes, France, [5]LSCE, CNRS, CEA, Gif-sur-Yvette, France, [6]LGO, CNRS, IUEM, Université de Brest, Plouzané, France, [7]Research Center for Geotechnology, Indonesian Institute of Sciences, LIPI, Bandung, Indonesia

**Key Points:**
- Probabilistic evaluation of reef carbonate production
- Reef productivity primarily dictated by glacial cycles, uplift, and subsidence
- Quaternary coral reefs modulate the chemical budget of oceans and atmosphere

**Supporting Information:**
- Supporting Information S1
- Video S1
- Video S2

**Correspondence to:**
L. Husson,
laurent.husson@univ-grenoble-alpes.fr

**Citation:**
Husson, L., Pastier, A.-M., Pedoja, K., Elliot, M., Paillard, D., Authemayou, C., et al. (2018). Reef carbonate productivity during Quaternary sea level oscillations. *Geochemistry, Geophysics, Geosystems*, *19*. https://doi.org/10.1002/2017GC007335

Received 10 NOV 2017
Accepted 11 MAR 2018
Accepted article online 30 MAR 2018

**Abstract** Global variations in reef productivity during the Quaternary depend on external parameters that may alter the global chemical balance in the oceans and atmosphere. We designed a numerical model that simulates reef growth, erosion, and sedimentation on coastlines undergoing sea level oscillations, and uplift or subsidence. We further develop a probabilistic evaluation that accounts for variable vertical ground motion, erosion, and foundation morphologies. *Absolute* sea level change appears primordial, as productivity must have increased by an order of magnitude since the onset of the glacial cycles, ~2.6 Ma. But most important is *relative* sea level change, i.e., eustasy modulated by uplift or subsidence, that rejuvenates the accommodation space and exposes pristine domains of the shore to active reefs at each cycle. Integrated over the long-term, vertical land motion sets the pace of reef growth: productivity in tectonically unstable domains is thus expected to be up to 10 times higher than in stable regions, if any. We quantify the global length of reef coasts and the probability density functions for slopes and uplift rates. Productivity waxes during transgressions to reach 2–8 Gt $CaCO_3$/yr and wanes during highstands, which may contribute to increase atmospheric $pCO_2$ by several tens of ppm during deglaciations. Over the last 1.5 Ma, reefs precipitated ~$0.8 \times 10^6$Gt $CaCO_3$ (~$500 \times 10^3$ $km^3$), the equivalent of a 1 m-thick layer spread over the entire surface of the Earth. This production modulates the calcium budget, for it represents some 30% of the modern Ca flux in the ocean.

## 1. Introduction

Worldwide, coral reefs cover a surface of ~250,000 $km^2$ (Figure 1a) and grow at a characteristic rate of a few mm/yr, therefore constructing extensive carbonated edifices, that essentially parallel tropical coastlines. Because they did similarly throughout the course of Late Cenozoic sea level oscillations, they have left fingerprints in the landscape in the form of staircase sequences of drowned or emerged (Figures 1b–1e) fossil reefs. The production rate, however, adjusts to the temporal variability of the settings. Because coral reefs simultaneously alter the carbon and calcium budgets, they impact the chemistry of the oceanic and atmospheric reservoirs (as for instance explored for the last deglaciation; Opdyke & Walker, 1992; Vecsei & Berger, 2004; Ware et al., 1992). Deriving such metrics from a comprehensive collection of direct measurements is out of reach and we therefore rely on the predictive capacity of numerical models. Our purpose is to quantify, beyond the Holocene, throughout Mid to Late Quaternary glacial cycles, the variations in the worldwide productivity of reef carbonates, and to provide a quantitative basis to evaluate their contributions to the chemical cycles.

We particularly focus on the roles of absolute sea level change, uplift or subsidence, and wave erosion that set the pace of reef construction, destruction, and sedimentation, at a global scale, but are seldom considered. This approach does not rule out the prominent role of intrinsic parameters (light of course, but also salinity, turbidity, temperature, organic matter content, $pCO_2$, etc.) on local reef growth (see e.g., Falter et al., 2013; Montaggioni, 2005). But such modulations presumably cancel out at a global, statistically representative scale, namely that of the intertropical zone (Figure 1), and only extrinsic processes can globally modify the productivity of tropical shallow-water carbonates—thereafter referred to as *coral reefs*. Overall, the prominent process operating on instantaneous reef productivity is certainly sea level oscillations (e.g.,

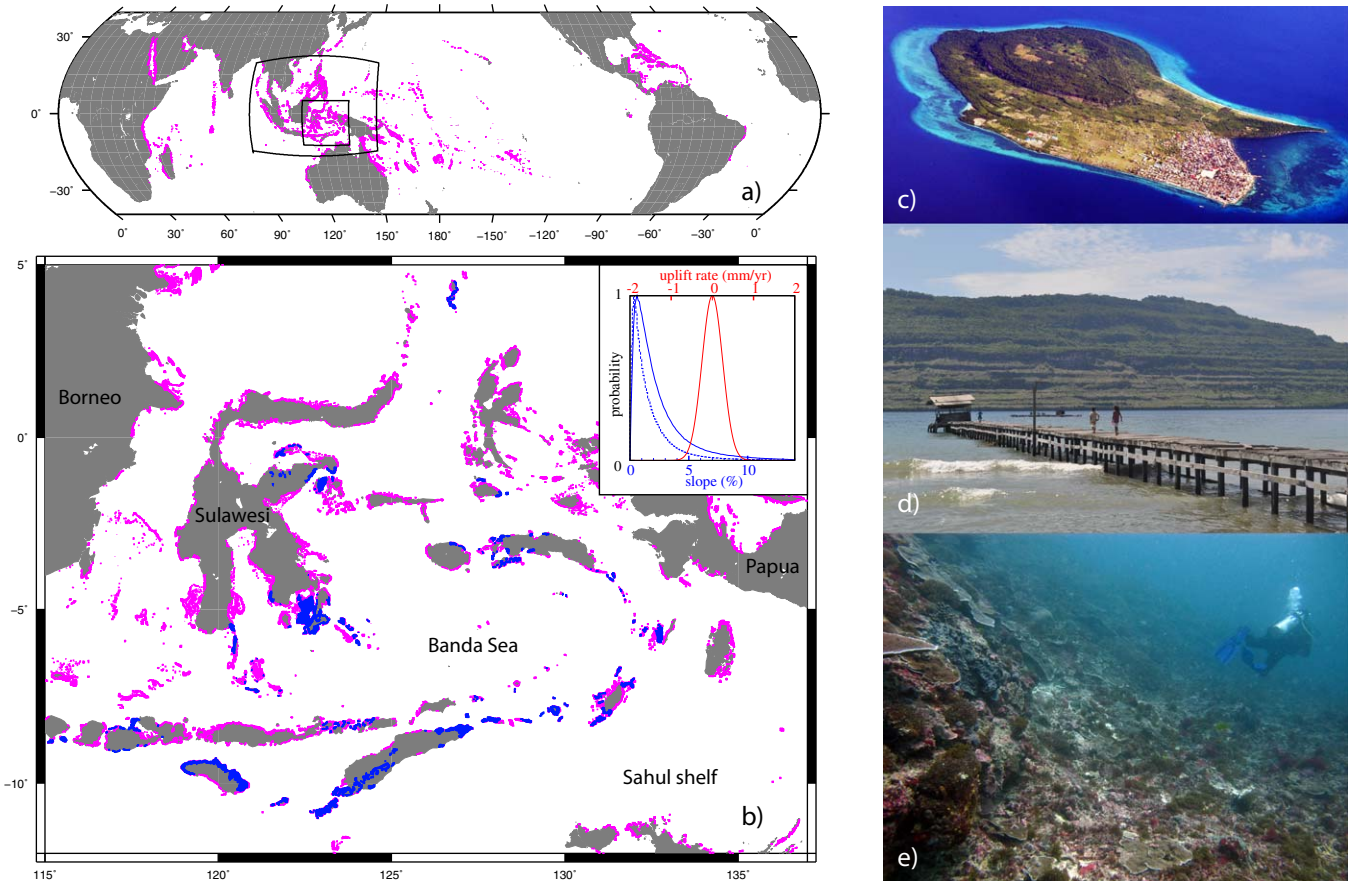


**Figure 1.** The coral world. (a) General map (boxes surround SE Asia—large box—and Wallacea—small). (b) Wallacea. Modern shallow-water reefs in magenta (after Burke et al., 2011), Pleistocene reefs in blue (from the 1:250,000 geological maps of Indonesia). (inset) Probability density functions for slopes (blue) and uplift rates (red) in Wallacea only (solid) and SE Asia (dashed), as defined in Figure 1a (see section 6.1). (c) Aerial photograph of Telaga Kecil, SE Sulawesi, displaying a flight of Late Cenozoic reefs and a modern fringing reef circumscribing the sequence. (d) Emerged sequence of Late Cenozoic reefs in Buton island, SE Sulawesi. (e) Submerged fossil strandline at −20 mbsl depth, Bali.

Montaggioni, 2005). But throughout the Quaternary, other extrinsic factors affect reef accretion and productivity. Tectonics affects both the relative sea level rates of change and the shape of the substratum: over long time scales, uplift or subsidence makes available different substrate morphologies to reef growth. Another parameter is the morphology of the underlying foundations (e.g., Neumann & Macintyre, 1985). On a short time scale (less than that of a glacial cycle) that space is controlled by the morphology of the anterior reef units. On longer time scales, it is the mean slope that defines the morphologic evolution of the substratum, for it encapsulates all shorter time scale events. Last, coastal erosion redefines the morphology of the substratum and redistributes the eroded products as sediments. Among those factors, sea level oscillations during the glacial cycle are specific to the Plio-Quaternary, while uplift or subsidence, and erosion are not as clearly time dependent.

In order to achieve a comprehensive understanding of these interactions, they need to be examined at two time scales to quantify how they foster or curb the dynamics of reef systems: on the short term—that of a unique glacial oscillation, and integrated over several glacial cycles, typically the Pleistocene. First, at short time scale (1–10 kyr), reef productivity is thought to be instantaneously controlled by the rate at which sea level fluctuates, and the various short-term behaviors are covered by the concepts of *keep-up*—when accretion rates meet sea level rise, *catch-up*—when reefs recover after a period of stunted growth in the photic zone, and *give-up*—when reefs cannot afford to keep-up with sea level rise and drown (Neumann & Macintyre, 1985). Second, on the longer, Late Cenozoic time scale, we similarly hypothesize that the onset of the glacial cycle as well as the variations of its amplitude and frequency possibly modulated the overall behavior, and productivity of coral reefs. Early Pleistocene glaciations (prior to ∼1,100 ka) were dominated by

lower amplitudes of sea level change (typically 60 m), shorter periods (41 kyr) oscillations—the *40 kyr world*, during which cycles last for one obliquity cycle. More recent cycles (later than 600 or 400 ka) mostly feature high amplitude (typically 120 m), high periods (100 kyr) oscillations—the *100 kyr world*, where the dominating cycles last two or three obliquity cycles. Following the Mid-Pleistocene Transition (typically 1,100 ka to 600–400 ka, but bracketing ages are not consensual because of its transitional nature) was the onset of the major phases of development of the prominent barrier reefs (possibly the Great Barrier Reef (Alexander et al., 2001; Braithwaite et al., 2004; Webster & Davies, 2003), the Risku Barrier Reef (Yamamoto et al., 2006), the Florida Keys (Multer et al., 2002), and New Caledonia Reef (Cabioch et al., 2008; Montaggioni et al., 2011). It is tempting to envision the blooming of these major reef systems as caused by the west changing pace of sea level oscillations (Montaggioni & Braithwaite, 2009; Yamamoto et al., 2006).

Direct measurements of reef productivity on sedimentary cores (see Dullo, 2005, for a review) are commonly used to unravel past rates of sea level change. Yet because they require heavy analysis, they remain too sporadic to be statistically representative (the response vary across reef systems, see for instance Camoin and Webster (2015)) and do not permit to draw generic behavior laws for reef systems. In the absence of such database, globally tested models are a promising alternative (as outlined in recent reviews, Braithwaite, 2016; Camoin & Webster, 2015; Montaggioni & Braithwaite, 2009; Woodroffe & Webster, 2014). Models that are calibrated on local observations successfully permit to overcome this issue (e.g., Barrett & Webster, 2012; Harris et al., 2015; Montaggioni et al., 2015). We take advantage of the predictive power of numerical models to extrapolate and yield quantifications that are otherwise out of reach. We do not aim for a collection of well-documented but isolated, particular cases. Instead, our analysis is based on the theoretical grounds of a numerical model (that derives from observations) in order to comprehensively assess the global response of reef systems to a variety of forcings.

We thus numerically modeled and computed the productivity of coral reefs undergoing a variety of scenarii, accounting for sea level oscillations, variable uplift and subsidence rates, slopes, and erosion rates, toward a probabilistic assessment of the impact of each process. We first analyzed how reef productivity responds to sea level change on the glacial cycle time scale and integrated it throughout the Pleistocene. We then quantify the extent to which extrinsic parameters—namely uplift, subsidence, and erosion rates—foster or curb reef productivity. Our results are subsequently applied in a probabilistic framework, to quantify the bulk contributions of coral reef sources to the chemical budget. We gradually quantify reef production by zooming out from Wallacea (the eastern part of SE Asia, where reefs are extremely prolific), to SE Asia and to the entire intertropical zone (Figure 1). Last, we take advantage of our probabilistic analysis to quantify the associated potential impact on the Ca and $CO_2$ budgets during the Late Quaternary by applying our results to SE Asia, and to the entire intertropical zone. Our analysis provides an unprecedented evaluation of the amount of carbonate that were sequestrated, reworked, and released by coral reefs over the middle and upper Pleistocene.

## 2. Modeling Reef Production

Numerical models attempt to reproduce the morphology of emerged or submerged sequence of fossil coral reefs (e.g., Bosscher & Schlager, 1992; Koelling et al., 2009; Toomey et al., 2013; Turcotte & Bernthal, 1984; Warrlich et al., 2002). We developed a 2-D Fortran numerical code that accounts for depth-dependent reef growth rates, erosion, and sedimentation (available upon request). At any location on the profile, the reef growth module assigns a slope-normal growth rate vector. This implies that a vertical component of reef growth adjusts to sea level at all times, but also that a lateral component of reef growth ensures that the reef coevally progrades whenever appropriate conditions are met. This rate $G$ (see Parameters and Symbols Table 1) is defined as a fraction of the growth potential rate $G^*$, which is the maximal rate at which the reef system grows under optimal conditions. This optimal rate is systematically hampered by the local settings. Penalties apply, such that

$$G = \gamma\, \zeta\, G^*. \tag{1}$$

$\gamma$ is the depth-dependent penalty coefficient, which corresponds to the waning of the photic zone down to depth $z_{max}$ (unlike the tanh function, as in Bosscher and Schlager (1992) or Koelling et al. (2009), we ignore minor contributions at greater depths, that are embedded in the sediments—see below), such that

**Table 1**
*Parameters and Symbols*

| Symbol | Definition | Value and unit |
|---|---|---|
| $G^*$ | Reef growth potential | 12 mm/yr[a] |
| $z_{ow}$ | Minimal depth for the open water | 2 m |
| $z_{max}$ | Maximum reef growth depth | 10–50 m |
| $z_{min}$ | Optimal reef growth depth | 1 m |
| $\gamma$ | Vertical reef growth penalty coefficient | |
| $\zeta$ | Horizontal reef growth penalty coefficient | |
| $E^*$ | Erosional potential | $10^{-2}$ to $3\times 10^{-2}$ m$^3$ yr$^{-1}$ [$2\times 10^{-2}$ m$^3$ yr$^{-1}$] |
| $z_0$ | Reference depth for wave action | 4 m |
| $K$ | Coefficient of erodibility | 0.1 (bedrock)/1 (notch) |
| $\theta$ | Critical sediment slope | 10° |
| $\alpha$ | Initial slope | 1%–50% [4%] |
| $U$ | Uplift rate | −2 to 2 mm/yr [0 mm/yr] |

*Note*. Bracketed values denote the reference case.
[a]Note that the potential rate is a theoretical maximal rate, seldom achieved in natural environments.

$$\gamma = \frac{1}{2}\left(1+\cos\frac{\pi h(s)}{z_{\max}}\right), \tag{2}$$

where $h(s)$ is the local depth along the curvilinear profile. At shallower depths than $z_{min}$ (the shallowest few meters where waves are active), the penalty coefficient linearly decreases to 0 at the surface. This threshold ensures that maximal production occurs at depths of $z_{min}$ and below (because the cosine function gently declines at shallow depths), but not above it. The distance to the open ocean (as defined by the location of first occurrence of minimal water depth $z_{ow}$, scanning landward) is also quantified and plugged into the penalty factor $\zeta$, such that

$$\zeta = \frac{1}{2}\left(1+\tanh\left(\frac{x_{ow}-x}{\delta}\right)\right), \tag{3}$$

where the tension $\delta$ sets the rigidity of the function. We introduce this parametrization, which is not found in earlier models, to account for the focused reef growth at the reef crest. Landward, this penalty ensures that the production is focused at the reef crest; this represents the joint effects of the landward increasing turbidity and of high levels of oxygenation that are conducive to coral development. Oceanward, its effect is most often superseded by the vertical penalty function, but also by the fact that the model systematically chops unrealistic overhanging reefs. Only when the topography at greater depths than $z_{ow}$ declines very gently does the tanh play a role and ensures a gradual transition toward the open water and greater depths. In practice, these penalty coefficients $\alpha$ and $\gamma$ impose that $G$ is seldom close to $G^*$.

In our model, coastal erosion is designed to effectively account for the joint effects of chemical, mechanical, biological erosion on the seabed, notch carving at sea level followed by the collapse of overhanging material, sea cliff formation, and carving of a rocky shore platform. The erosion module sets the erosion potential to a fixed power, that we express as a volume per unit time $E^*$. That erosional volume is dispatched along the profile as a function of depth, from the seaward edge shoreward. The remainder of the erosional power $E_r$ gradually decreases as energy gets dissipated on the seafloor, such that

$$\frac{\partial E_r}{\partial s} = K\,E_r \exp\left(-\frac{h(s)}{z_0}\right), \tag{4}$$

where $z_0$ is the typical depth of wave action, and $h(s)$ is the local depth along the curvilinear profile, and $K$ a coefficient of bedrock erodibility. At each location, the erosional power is a fraction of $E^*$, expressed as an incremental eroded volume per unit time. Erodibility linearly depends on the remaining erosional power. On the seabed, it exponentially decreases as a function of depth, becoming negligible at depths greater than $z_0$. At the shoreline, when the profile becomes exposed, the remaining power $E^* - \int_s \frac{\partial E_r}{\partial s}\,ds$ serves to undermine the coast and carve 1 m high notches. The overhanging material above the notches instantaneously falls apart and active sea cliffs form. Erosion of exposed material is assumed negligible. This minimizes the estimated oceanward flux of calcium carbonate to an unknown extent, but the temporal

persistence of pristine staircase sequences in tropical landscapes (e.g., Haiti, Barbados, Red Sea, Indonesia, Papua, and Philippines) plead for a modest contribution compared to seabed erosion and shore cliff carving (see Figures 1c and 1d).

In our simulations, we tested the impact of erosional power $E^*$, that we alternatively set to $10^{-2}$, $2 \times 10^{-2}$, and $3 \times 10^{-2}$ $m^3\,yr^{-1}$, per unit length. In practice, these values were arbitrary chosen because they compete with reef growth rates, without overcoming the reef growth potential, as observed in most natural landforms, where both erosional platforms and fossil reefs remain (as observed at many locations, for instance in Sumba island (Pirazzoli et al., 1991) and elsewhere in Indonesia (Molnar & Cronin, 2015), the Barbados (Speed & Cheng, 2004)).

The eroded volume from the seabed and the shore is then imported into the sedimentation module that simply deposits the equivalent volume immediately seaward, with a critical stability slope (set to 10°) on the reef foot. Lagoons or depressions are filled up before the remaining volume flows further seaward.

Sea level oscillations, initial slope, and vertical ground motion are the forcing mechanisms. Absolute sea level (*asl*) oscillations are taken from the reconstruction of Bintanja and van de Wal (2008), over 1,500 kyr, whose reconstruction method, based on a continuous global sea level curve based on benthic oxygen isotope data, makes it suitable for modeling (Past Interglacials Working Group of PAGES, 2016). We arbitrarily ignore the many competing reconstructed sea level curves (see e.g., the compilation by Caputo (2007)) and do not consider any uncertainty, as we do not focus on the detailed timing of reef evolution. For the same reason, we do not impose a time-lag before reef growth resumes to its maximum growth rate (∼0.5 kyr, as in Koelling et al. (2009)). Instead, we analyze the theoretical response to the cyclicity, for which most curves agree upon. Relative sea level (*rsl*) curves are defined as the convolution of absolute sea level curve and vertical land motion (set to zero in the reference model, making *rsl* and *asl* identical). We explore a range of slopes $\alpha$ for the initial morphology, from 1 to 50% (1, 2, 4, 6, 8, 10, 15, 25, and 50%), that encompass most shorelines (besides uncommon, extremely steep slopes). Last, uplift and subsidence rates $U$ vary between $-2$ and 2 mm/yr (by 0.1 mm/yr increments between $-1$ and 1 mm/yr, completed by $-2$, $-1.5$, 1.5, and 2 mm/yr) and encompass most cases on Earth (Pedoja et al., 2011, 2014). They are kept constant throughout each simulation.

Overall, by varying the erosional power $E^*$, the initial slope $\alpha$ and the uplift and subsidence rate $U$, we ran 675 models. Of course, all functions that control reef growth, erosion, and sedimentation could be additionally tuned and tested at will, but we essentially focus on the parameters and leave the intrinsic parametrization unchanged. In the following simulations, $G^*$ is fixed to a rate of 12 mm/yr. In practice, this apparently high value is almost never met but it is instead chosen to yield mean actual rates that compare to observations (about half this rate or less, as compiled in Dullo (2005) and Montaggioni and Braithwaite (2009)). This choice does not alter significantly our results, simply because actual growth rates (at given space and time step) vary much more efficiently than $G^*$ (see below). Varying $G^*$ would thus only add apparent complexity. The sine function for the vertical penalty sets production to zero at 20 m (thus neglecting the actual minor accretion rates beyond that depth). The horizontal penalty is defined such that the minimal water depth $z_{ow}$ and tension $\delta$ are set to 2 and 15 m, respectively, so that 75% of the decline in potential growth rate takes place over a distance of ∼30 m at the ridge crest in most cases. Erosion is constrained with $z_0 = 4$ m, which maintains low erosion rates below that depth. The profile is additionally marked by an erodibility factor set to 0.1 offshore and to 1 onshore.

We analyze our results with respect to a reference model, where $U = 0$ mm/yr; $E^* = 2\ 10^{-2}$ $m^3\,yr^{-1}$; $\alpha = 4\%$. The main outcome of most previous models (e.g., Koelling et al., 2009; Toomey et al., 2013; Turcotte & Bernthal, 1984; Warrlich et al., 2002) is a prediction for the present-day morphology of a reconstructed sequence of reef bodies, an output that our model yields too (Figure 2 for the final situations; online animations in supporting information for their animated time evolutions). Our model finely predicts existing morphologies but we here set aside the geometrical aspects and instead focus on the carbonate productivity. This metric, that we compute at each time step, differs from the accretion rate (in mm/yr, as in Dullo, 2005), which ignores the width of the reef expanse. Instead, reef productivity (in $m^3/yr$) is the volume of precipitated carbonated reef per unit time and per unit length of coastline.

Of course, our 2-D numerical model simplifies the complexity of reef systems in a tractable way so as to capture the processes at play and quantify their respective contributions. This conceptual model thus ignores

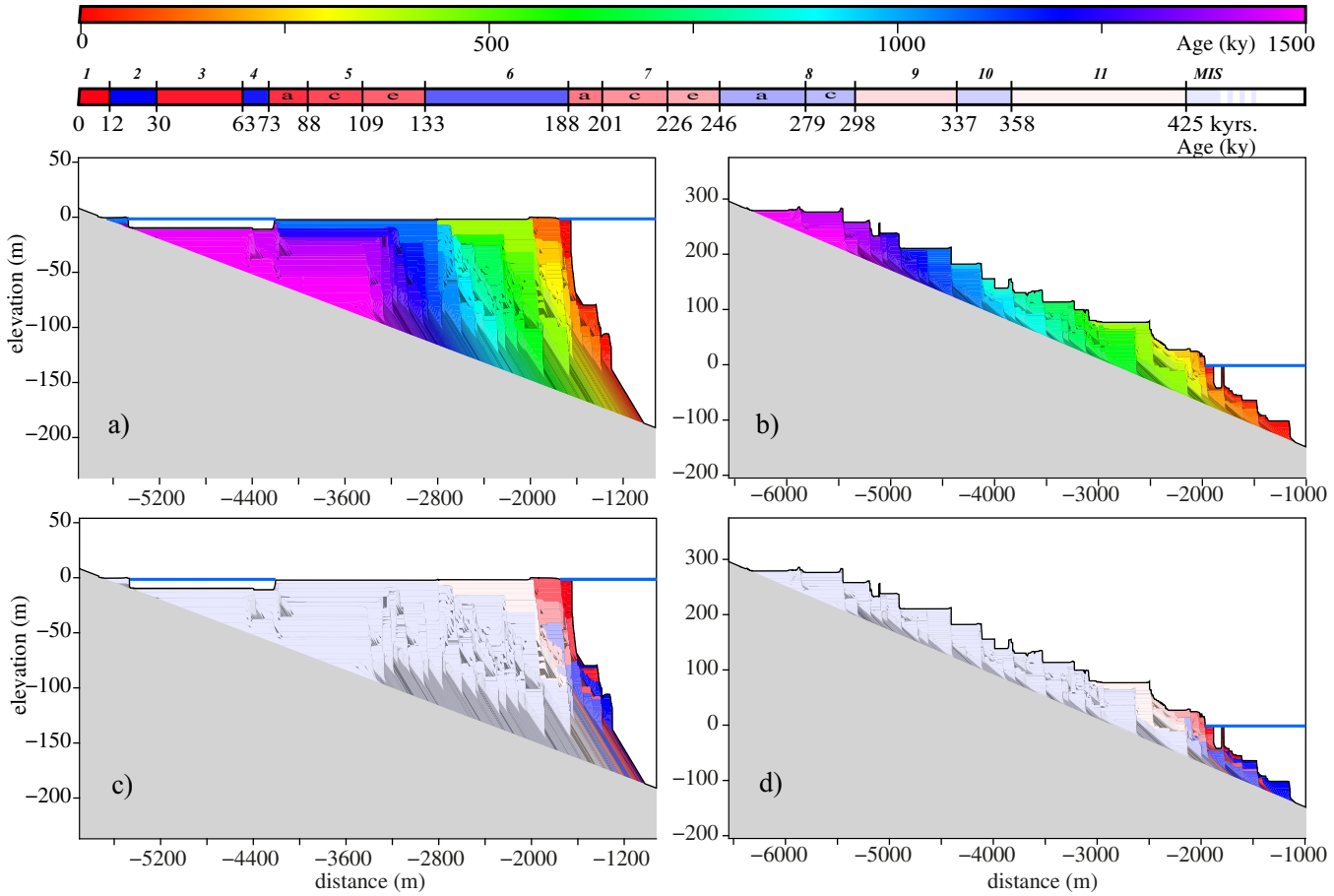


**Figure 2.** Typical modeled reef architectures. (a) Reference model ($U = 0$; $E^* = 2 \times 10^{-2}$ m$^3$ yr$^{-1}$; $\alpha = 4\%$) and (b) representative geometry for random case ($U = 0.2$ mm/yr; $E^* = 10^{-2}$ m$^3$ yr$^{-1}$; $\alpha = 8\%$). (c, d) Same models with calendar (rainbow) and glacial cycle (polar) scales as defined by their Marine Isotopic Stages (MIS), and focused over stages MIS11–MIS1. Saturation gives age, hue denotes glacial (blue) and interglacial (red) stages.

perturbations caused by the many physical and biological controls of reef growth (see e.g., Falter et al., 2013). We do not rule out their local effects at a local scale but simply assume that they cancel out from a statistical standpoint.

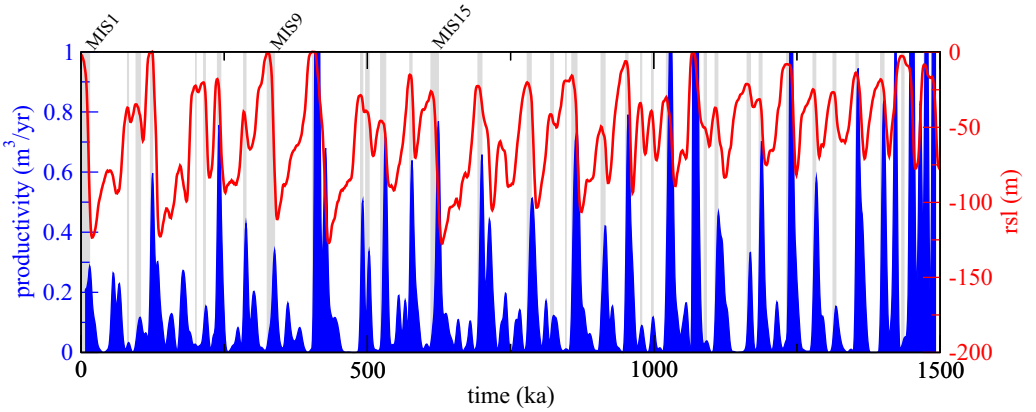


**Figure 3.** Modeled reef productivity for reference model (blue, $U = 0$; $E^* = 2 \times 10^{-2}$ m$^3$ yr$^{-1}$; $\alpha = 4\%$), eustatic sea level curve (red, Bintanja & van de Wal, 2008), and peak to peak time offset (gray) between time of maximum sea level stands (higher than −50 m) and time of predicted maximal productivity.

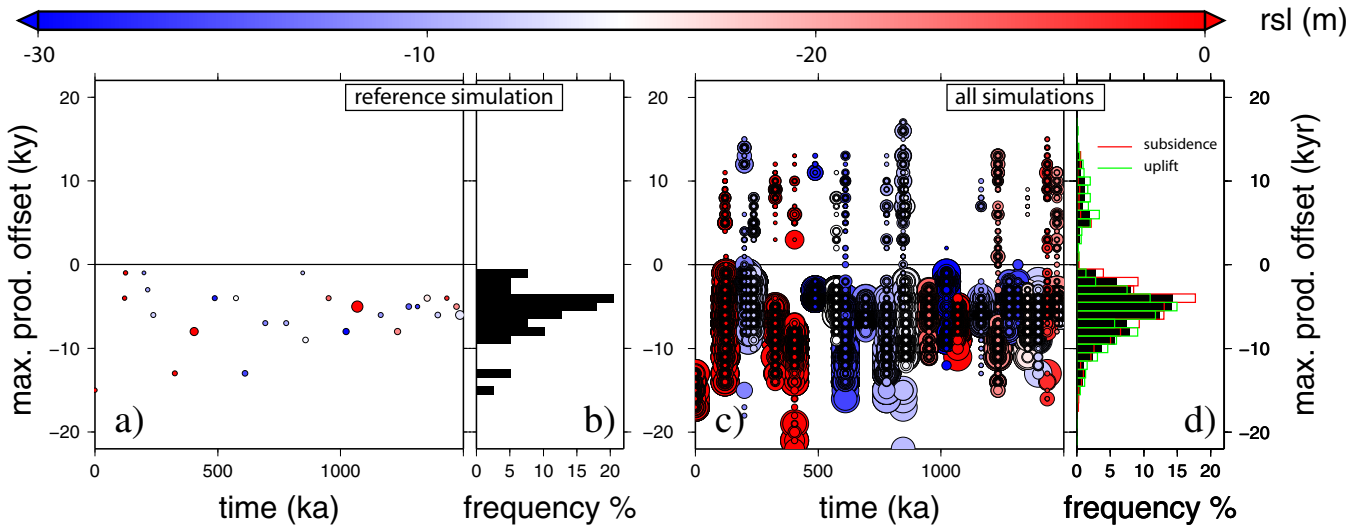


**Figure 4.** (a) Time offset between maximum sea level stands and maximal productivity as a function of time, relative sea level maximum (color coded), and peak productivity (symbol size), for the reference case (as in Figure 3). (b) Frequency distribution, reference case. (c) Time offset between maximum sea level stands and maximal productivity as a function of time, relative sea level maximum (color coded), and peak productivity (symbol size), for all cases. (d) Frequency distribution, for all cases (black, average offset −5.9 kyr), for uplift only (green, average offset −6.4 kyr), and for subsidence only (red, average offset −5.4 kyr).

## 3. Reef Production During the Glacial Cycle

Reef productivity responds to sea level change (e.g., Neumann & Macintyre, 1985). Our simulations track the variable productivities during Pleistocene sea level oscillations, but in addition provide insights on the growth regimes as a function of relative rate of sea level change.

### 3.1. Reef Productivity During Sea Level Oscillations

The periodic response in productivity of the reef is shown in Figure 3 for the reference model ($U = 0$; $E^* = 20$; $\alpha = 4\%$). Productivity and relative sea level oscillate at the same frequency: each peak in sea level oscillation is accompanied by a peak in productivity (up to ~1 $m^3/yr$), which decreases to almost zero in between sea level highstands. Sea level and productivity peaks are not strictly coeval, and the offset (brown bars, Figure 3) is systematically negative (Figure 4), which means that productivity peaks predate sea level highstands. Productivity reaches its maximal value on average 4–5 kyr before the eustatic maxima, i.e., when sea level rises at the fastest rate, and constantly promote reef building by constantly and efficiently rejuvenating the accommodation space. In this case, three outliers (for Marine Isotopic Stages MIS1, MIS9, and MIS15) show particularly premature peak productivities, shortly after the preceding lowstand. Peak productivities remain fairly uniform throughout, with a mean rate of 0.52 $m^3/yr$ (mean sea level highstands peak at −22 m). Two outliers, at 404 kyr (MIS11) and 1,070 kyr (MIS 31), correspond to periods with larger highstands relative to the rest of the record. During these two periods, sea level reached pristine domains of the coast, where no earlier reef body fills in the accommodation space. Lowstands, conversely, do not postdate, nor predate, periods of fostered productivity. The reasons of this contrasted behavior are discussed below.

This exercise can be expanded to all simulations covering the range of representative (see above) uplift and subsidence rates, slopes, and erosional power (Figure 4). Results are comparable to the reference case: predicted peak productivities almost systematically predate sea level highstands, by about 5 kyr on average, with a standard deviation of about 3 kyr. Whenever peak productivities postdate sea level highstands, their values are systematically lower than when they predate. Such observations are consistent with, for instance, observations from MIS5 on Barbados (Blanchon & Eisenhauer, 2001). Similarly, Pacific reefs grew quickly ~2 kyr before the Holocene eustatic maximum (Murray-Wallace & Woodroffe, 2014). Again, the offsets for some stages are larger than for other and exceed the 5 kyr mean. This is the case of MIS11, where the offset is larger than for any other Isotopic Stage, by several kyr (from 5 to 22 kyr); this is possibly due to the fact that deglaciation lasts slightly longer and is deprived of second order substages, but also to the specific geometry of the foundations at that time, after earlier cycles shaped it, either by construction or erosion.

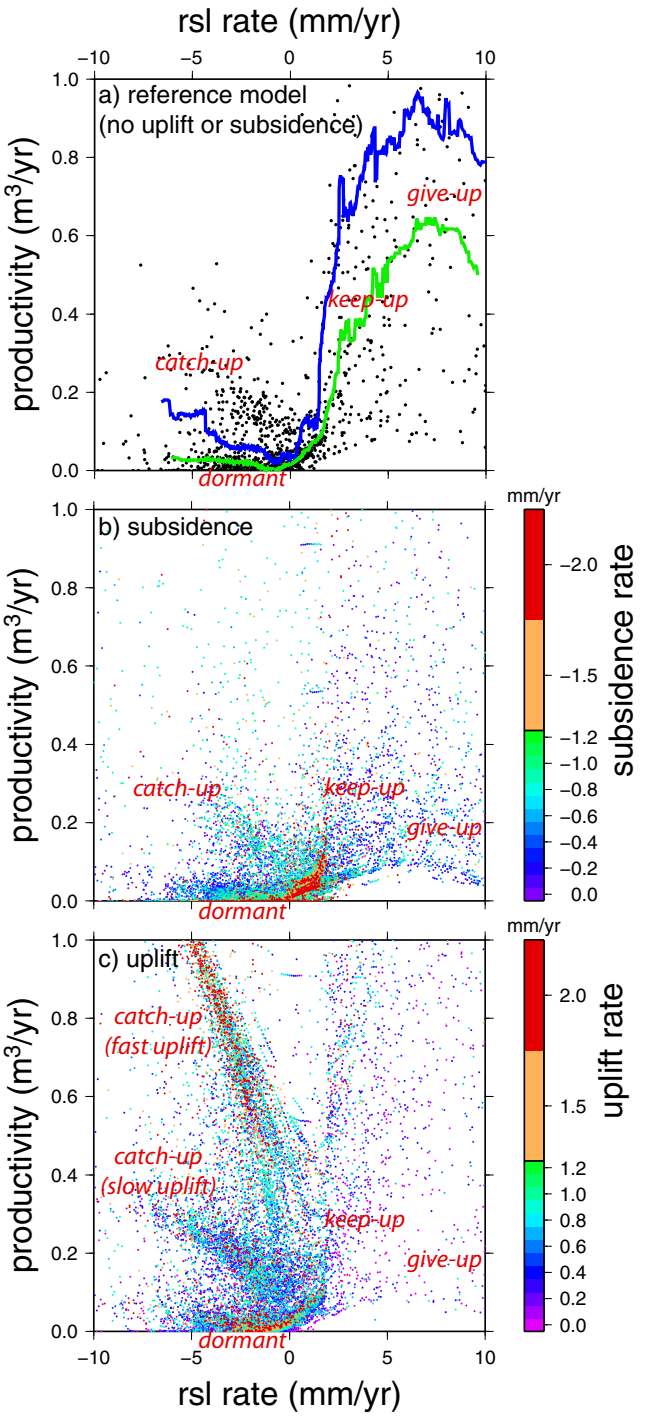


**Figure 5.** (a) Instantaneous reef productivity as a function of the rate of relative sea level change (positive values indicate sea level rise), median and average curves (green and blue, 100 data points sliding bins) sampled every 1 kyr, for reference parameters ($E^*=2\times10^{-2}$ m$^3$ yr$^{-1}$; $\alpha=4\%$) in the absence of uplift or subsidence ($U=0$). (b) Instantaneous reef productivity as a function of relative sea level change, sampled every 1 kyr, for reference values ($G^*=12$ mm/yr; $E^*=2\times10^{-2}$ m$^3$ yr$^{-1}$; $\alpha=4\%$), but allowing for variable subsidence rates. (c) Same as Figure 5b, but allowing for variable uplift rates.

Interestingly, the offset between the timing of peak productivity and highstands is shorter by ~1 kyr for subsiding models than for uplifting models (Figure 4d): average values for offsets that precede sea level highstands are −6.4 kyr (uplift only), −5.4 kyr (subsidence only), and −5.9 kyr (all simulations). This is due to the fact that, given our parametrization, periods of relative sea level stagnation are accordingly delayed (subsidence) or anticipated (uplift) by vertical ground motion, by ~1 kyr with respect to *absolute* eustatic timing.

### 3.2. Carbonate Productivity and Relative Sea Level Rate of Change

Coral reefs precipitate carbonate at variable rates that are controlled by the relative change in water depth forced by sea level change and vertical ground motion (Figures 2c, 2d, and 3). The fact that they jointly vary mirrors the primordial influence of relative sea level change rate. More precisely, it reveals how the accretion regime adjusts to relative sea level change (in addition, of course, to other intrinsic factors such as nutrient levels, water turbidity, and many others; Falter et al., 2013). Reef behavior is extremely contrasted between periods of sea level rise and periods of sea level fall, as exemplified by the reference model (Figure 5a). The reference model is conform and shows variable regimes. At low transgression rates (up to ~7 mm/yr), productivity follows in a *keep-up* regime (as shown Figure 5a, by both the mean and median curves). Productivities in this regime are highly variable, and reach the highest values of the simulations. These events of fostered productivities correspond to periods of reflooding window (Jorry et al., 2010) during glacial terminations. Productivity declines at higher rates, progressively approaching the *give-up* regime. However, actual *give-up*, for which rates decline to zero for persistent time periods, only occurs at faster rates. At rates lower than 2 mm/yr instead, *give-up* is often not sustained and the *catch-up* regime supersedes it. Regressions show two contrasted arrays, either entering a low productivity regime or slightly higher productivities. We refer to the first regime as *dormant*, during which it only lays a slim veneer of reef carbonate over the antecedent substratum. The second array shows a more fertile behavior during regressions; reef production reaches higher rates that can be explained by the *catch-up* regime of reefs that have *given up* during the preceding transgressions and resume their expansions when the water level shallows. This behavior is less frequent than the *dormant* regime, as shown by the median curve that remains much lower than the mean curve. Note that the *catch-up* regime also occasionally occurs during periods of transgression when rates of sea level rise decrease, which may explain the dispersion of the signal in the transgressive domain in Figure 5a.

Because relative sea level rate of change is primarily dictated by sea level oscillations (as opposed to vertical ground motion), this behavior has implications on the productivity during glacial cycles. Fast relative sea level change (absolute sea level change and vertical land motion) mostly stimulates the productivity in the *keep-up* and *catch-up* regimes. The end-member, in the absence of any sea level change, yields minimal, almost null, productivities. In practice, lateral reef growth often prevents productivity from reaching null rates, as observed in many natural systems (Scoffin & Tissier, 1998). Major implications arise on the long term, for it predicts that the overall

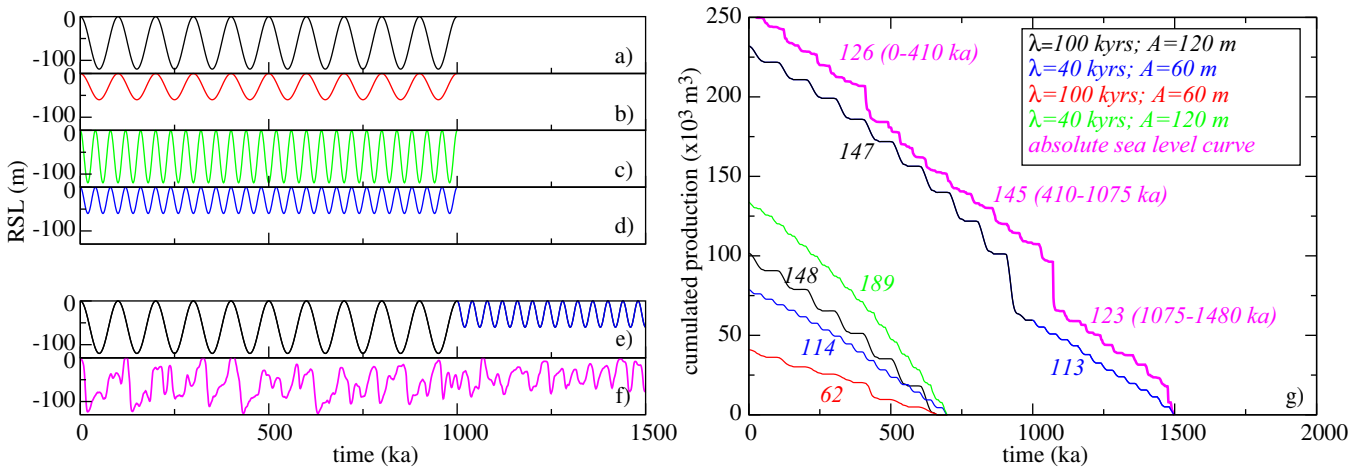


**Figure 6.** (left) Synthetic input sea level curves (a–f) with variable amplitudes (60 and 120 m) and periods (100 and 40 kyr). (f) Reconstructed sea level curve from Bintanja and van de Wal (2008). (g) Cumulative reef production (numbers in italic are productivities in $m^3\ kyr^{-1}$). Initial stages are graphically cropped at 1,500 kyr to discard the effect of initial conditions—the morphology of the foundations in particular.

productivity of reefs increased dramatically since the onset of the glacial cycle, and throughout the Pleistocene when the glacial cycle evolved until present day.

## 4. Response of Reef Productivity to the Changing Pace of Sea Level Oscillations During Pleistocene

Reef productivity also responds to relative sea level variations at lower time scales than the Pleistocene, and thus one expects the large frequency variations of sea level oscillations over the Mid-Pleistocene Transition *MPT* (Figure 3, after Bintanja & van de Wal, 2008) to significantly impact reef productivity. In order to test the sensitivity of reef productivity to the frequency and amplitude of sea level oscillations, we modeled the response to synthetic sea level curves of variable periods (100 and 40 kyr), amplitudes (60 and 120 m), and combination thereof, that are typical of the Pleistocene (Figure 6). All other parameters are held fixed as in the reference model ($U = 0$; $E^* = 2\times 10^{-2}\ m^3\ yr^{-1}$; $\alpha = 4\%$).

The computed productivity varies by a factor of 3 between the long period/short amplitude ($\lambda = 100$ kyr, $A = 60$ m) and the short period/high amplitude ($\lambda = 40$ kyr, $A = 120$ m) oscillations (Figure 6). Most productive regimes correspond to oscillations at large amplitudes, simply because when the accommodation space is greater ($A = 120$ m instead of 40 m), it leaves more room for sustained coral development. Such configuration does not make the reef thicker, but its bulk volume is larger. Shorter periods of oscillations ($\lambda = 40$ kyr) also foster the productivity, albeit to a lesser extent. The response further varies when models are run for longer time periods, with adjoint series of variable frequencies and amplitudes. A simulation where sea level changes from ($\lambda = 40$ kyr, $A = 60$ m) until 1,000 ka, and ($\lambda = 100$ kyr, $A = 120$ m) until 0 ka predicts that production increases after 1,000 kyr, i.e., during the MPT. The curve obtained for the reference case using the sea level curve of Bintanja and van de Wal (2008) shows a slightly more complex pattern. Two productivity peaks (MIS31 at ~1,070 ka and during the MIS11 highstand, at 440 ka) outweigh the others (Figures 3f and 3g). These peaks illustrate that productivity is mainly depending on the history of a reef platform: prior to MIS31, sea level had not been this high for almost 400 ka (since MIS47). Thus all the reef platforms that have formed since MIS47 are being flooded at once. Similarly, MIS11 is the time when sea level reaches values higher than those of MIS31 for the first time in more than 600 ka. Again, a lot of inundated reef platforms form an ideal environment for massive carbonate production. In addition, the exceptionally slow and long-lasting rate of sea level rise from MIS12 into MIS11 (around 5 m/ka) creates optimal conditions for reef development. Subsequent interglacials are not as productive as MIS11 or MIS31 because sea levels remain lower than MIS11 sea level highstand, and thus need subsidence or erosion to create accommodation space. Although ages are controversial, several of the main barrier reefs possibly fully expanded around MIS11. This is possibly the case for the Great Barrier Reef (Alexander et al., 2001; Braithwaite et al., 2004; Webster & Davies, 2003), Risku Barrier Reef (Yamamoto et al., 2006), Florida Keys

(Multer et al., 2002), and New Caledonia Reef (Cabioch et al., 2008; Montaggioni et al., 2011). Similarly in the Red Sea, to our knowledge, no reefal geomorphic records older than ~400 ka have been described in a continuous sequence, to our knowledge (Pedoja et al., 2014). The production curve can be split into three regimes separated by the two productivity peaks. The first transition marks the onset of the MPT, during which higher amplitudes and longer periods of oscillation appear. This is accompanied by a predicted productivity increase of 18%, because the combination of various amplitudes and wavelengths create accommodation spaces that were not available to the prior oscillations. This regime holds until MIS11, therefore slightly after the end of the MPT, during which the productivity peaks to unprecedented values (*Mid Brunhes Event*), because of its large amplitude. In the 100 kyr world, productivity decreases to more modest values, by some 15%. Again, we interpret this result by the fact that the post MIS11 period is routinely dominated by ($\lambda = 100$ kyr, $A = 120$ m) oscillations. This leaves little possibility to expand over pristine accommodation space, as opposed to more transient regimes. This suggests that noise—here the convolution of variable wavelengths and amplitudes—is a prominent fostering parameter (as exemplified for instance by the MIS5e Yucatán peninsula reef, showing abrupt regime and production changes; Blanchon et al., 2009).

Overall, the modulating effect of changing frequencies and amplitudes of sea level oscillations on reef productivity might have been less than ~20% during the Mid to Late Quaternary. However, these results show that over the Cenozoic, the influence of the gradually increasing influence of sea level oscillations has constantly increased coevally. This implies that the onset of the glacial cycles, and the following increasing amplitudes of oscillations until present day, gradually stimulated, and potentially triggered—the fast productivity that prevails until present day. This is further illustrated by the relationships between productivity and relative sea level rate of change (see section 3.2 and Figure 5a).

## 5. Uplift and Subsidence, Erosion, and Morphology of the Foundations

Sea level change is likely the most widely recognized extrinsic control on reef growth (e.g., Montaggioni, 2005). However, other processes—namely vertical ground motion, coastal erosion, and morphology of the substratum—may play a significant role. Over the 1,500 kyr modeled time period, absolute vertical ground motion overall foster productivity (Figure 7). Production rates remain very low for low absolute vertical ground motion rates, but increase up to 10 times in uplift regime and much more in subsidence: uplift or subsidence expose pristine domains to reef growth and therefore, at all cycles, expand the accommodation space.

In addition, productivity inversely scales with slope: it is higher for shallow slopes than for steep slopes (which matches observations; Blanchon et al., 2014). Shallow slopes display wider accommodation spaces, before water depth exceeds the reef capacity. The fact that the productivity scales almost linearly with the slope indicates (though it does not imply) that the accommodation space is predominantly close to saturation most of the time, in other words, that the *keep-up* regime prevails (it in turns implies that model predictions could in principle be normalized by the slope).

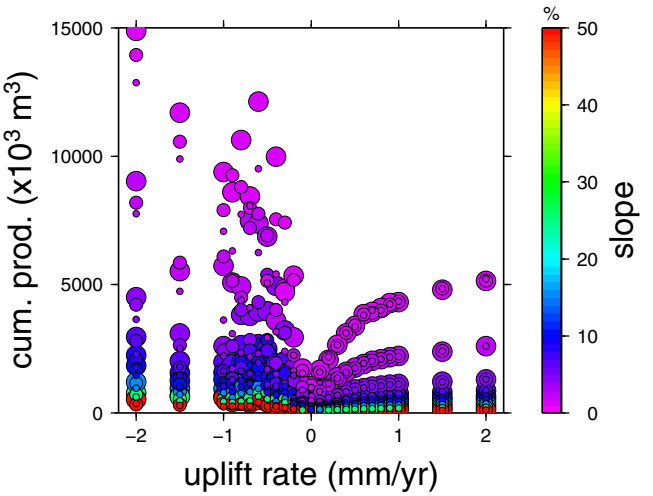


**Figure 7.** Bulk reef production over 1,500 kyr, per unit reef length, as a function of uplift rate, slope (color coded), and erosional power (small, medium, and large circles for $E^* = 1$, 2, and 3 $\times$ $10^{-2}$ m$^3$ yr$^{-1}$), for all simulations.

Furthermore, the behavior is bimodal. In uplift mode (Figure 7, positive values) results are well organized and production curves follow an array that is principally dictated by the slope, and where erosion plays a negligible role. Conversely in subsidence mode, results are more dispersed, because erosion alters the signal: domains that were previously eroded by wave action enter the accommodation space. In uplift mode conversely, those regions are gradually withdrawn from the system when reaching always more aerial domains. In other words, erosion modifies the shape of the substratum and thus the accommodation space in the subsidence mode, but not in the uplift mode. Thus, the cause is not the competition between rates of relative sea level change and vertical ground motion that is often an order of magnitude lower. It is the long-term rejuvenation of the accommodation space caused by subsidence or uplift that provides conducive grounds for more efficient reef development. The convolution of variable time scales is crucial: relative sea level has a determinant role on

the glacial cycle scale, while vertical ground motion is primordial at longer time scales. It is the joint effects of the two that sets the productivity of a given reef system tract.

The crucial impact of vertical ground motion appears even more strikingly when uplift and subsidence modes are treated in isolation, with all simulations considered (Figures 5b and 5c). Of course, transgressions (positive RSL rates) are more frequently associated to subsidence than regressions (negative rates), which are promoted by uplift. Regardless, the arrays of subsidence and uplift modes drastically differ. The main difference is that subsidence mode has a lower productivity during marine regressions (negative RSL rates) than uplift mode, where a strong array peaks to high values. This additional array is that of the fastest uplift rates. It corresponds to the *catch-up* regime that is boosted when uplift allows reef growth over deeper, pristine units. This array is thus dominated by fast uplift rates (predominantly higher than 1 mm/yr). At lower uplift rates (mostly lower than 1 mm/yr) during regression periods, two lower productivity arrays also appear in uplift mode and compare to similar arrays in subsidence mode, for similar absolute rates (lower than 1 mm/yr). The most productive array corresponds to the *catch-up* regime, both in uplift and subsidence modes, but over domains where the accommodation space was previously partly filled in during earlier cycles, which explains why the productivity is restricted. The lowermost array corresponds to the *dormant* regime, where the entire accommodation has been previously filled up. In both modes, during transgressive periods (positive RSL rates), productivity is never negligible. Wave erosion reshapes the foundation, and the reworked material reopens some accommodation space during transgressive periods. Conversely during regressions, eroded (or excavated) domains remain above sea level and do not contribute to reshape the foundations of the active reef system. This explains why in our models productivity can be null during regressions and never during transgressions. In both uplift and subsidence modes, transgressions (positive RSL rates) are dominated by the *keep-up* regime, up to RSL rates of approximately 5 mm/yr, and by the *give-up* regime for higher RSL rates. However, the transition is gradual and the 5 mm/yr rate is essentially indicative and shall not be regarded as a threshold.

## 6. Quantifying Reef Carbonate Production During Holocene and Pleistocene Times

Throughout the modeled period of time, the predicted productivity oscillates at the frequency of the cycles (Figure 3). The range of variation is considerable, from almost zero to several cubic meters per year, per unit length of coral reef. These variations thus impact the sediment yield of the oceans. One can quantify this contribution for a given region, provided local parametrization (slope, uplift rate, erosional power, etc.) can be made. In order to perform an integrated analysis, estimates of the total length of coastlines occupied by reefs, of slopes, and of uplift rates are requisite. We first focus on the Coral Triangle, and more specifically on Wallacea (roughly boxed Figure 1). Wallacea is at the heart of the Coral Triangle, bears the most spectacular reefs, and contains countless sequences of fossil reefs, whose vertical extent attests for uplift (Figure 1). The extensive distribution of coral reefs there, undergoing both uplift and subsidence, presumably makes it representative of most possible settings. We then expand our analysis to the entire intertropical zone (Figure 1).

### 6.1. Probabilistic Parametrization of the Mid to Late Quaternary Reef Environments

Because slopes and uplift rates are variable, and because their impact on reef accretion is high, we opt for a probabilistic evaluation of each figure. In order to get a representative distribution of slopes, we extracted all slopes of all islands of Wallacea from 90 m Digital Elevation Models (SRTM). For comparison, we extracted the slopes in the entire SE Asia (Figure 1). Assuming that the slopes immediately above sea level (between 0 and 100 m) are representative of the morphology of the substratum prior to the settlement of coral reefs, one retrieves the probability density functions (*pdfs*) for the foundation slopes (Figure 1). For Wallacea, some 50% slopes are lower than 2.5%, and only ~10% are larger than 5%. For the entire SE Asia (Figure 1), including the very shallow Sundaland platform, slopes are even shallower, but are typically concentrated over 1–2% (Figure 1).

Uplift rates in SE Asia greatly vary (see Evans, 1936 or Verbeek, 1908, for early observations, and Tomascik, 1997 or Wilson, 2011, for reviews), from the very fast rising Huon peninsula, Indonesian volcanic arc and subduction wedge, to the subsiding platforms of Sundaland (Doust & Sumner, 2007; Hanebuth et al., 2002; Wong et al., 2003). On the basis of the local estimates, of a global review on vertical ground motion (Pedoja et al., 2011, 2014), we propose a normal law (with an expected value of 0 mm/yr and a standard deviation of 0.25 mm/yr) for the probability density function of uplift rates in Wallacea (Figure 1).

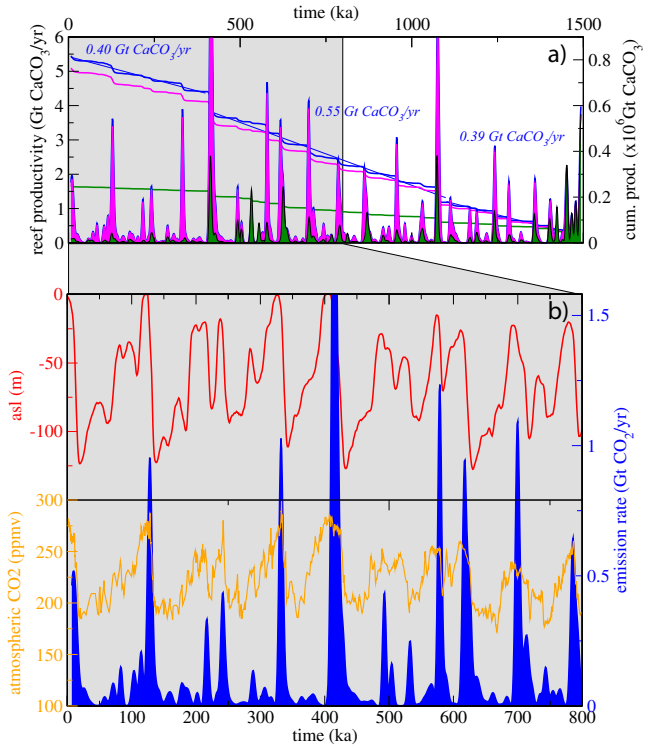


**Figure 8.** (a) World reef carbonate productivity (in Gt $CaCO_3$/yr) and cumulated reef production (in Gt $CaCO_3$). Magenta: expanding the probability density functions (*pdfs*) for slopes and uplift rates of Wallacea (Figure 1) to the entire intertropical zone. Green: in the absence of uplift or subsidence, but similarly expanding the *pdfs* for slope and uplift rates of Wallacea (Figure 1). Blue: expanding the *pdf* for SE Asia slopes (Figure 1). (b) Eustatic sea level (*asl* from Bintanja & van de Wal, 2008), atmospheric $CO_2$ (orange, after Lüthi et al., 2008), and modeled reef $CO_2$ emission rates integrated over the intertropical zone (blue, derived from the carbonate productivities shown in Figure 8a), for the last 800 kyr of $CO_2$ record.

Last, the total length of coastline that is actually occupied by reefs is an unavailable figure in the literature (as opposed to the surface they cover). We therefore approximated it by computing and integrating the perimeters of the modern reefs from a worldwide compilation map (see world map, Figure 1, after Burke et al., 2011) and dividing the sum by two (for perimeters account for both seaward and landward sides of reefs). Cumulated lengths are 73,000, 150,000, and 260,000 km for Wallacea, SE Asia, and the global intertropical zone, respectively. Wallacea only or SE Asia only account for a quarter, or a half, of the global reef length, respectively. Therefore, upon the approximation that the probability density functions of slopes and uplift rates of Wallacea are representative of the 260,000 km long intertropical reefal coasts of the World, we derive global estimates for carbonate reef production during the Mid to Late Quaternary. The purportedly most plausible case considers the *pdfs* of SE Asian slopes and uplift rates to be representative of the intertropical zone. For comparison, we computed the results in the case where the steeper slopes of Wallacea are representative, and in the case of absent uplift of subsidence (Figure 8a). Results show comparable results when either the slopes of Wallacea or those of SE Asia are accounted for, which suggests that the *pdf* for the slopes plays a negligible role, provided that it is based on a realistic sampling of intertropical slopes. In the absence of uplift or subsidence, productivity is significantly hampered, and the bulk production is decreased threefold (Figure 8a). This result confirms that uplift or subsidence is much more efficient than any other parameter in modulating reef productivity.

### 6.2. Carbonate Production

Integrated worldwide, over the 260,000 km long reef coasts, during the last glacial cycle, our models indicate that minimal production occurred during sea level fall, ~40 ka, and gradually resumed afterward to peak ~10 ka at a rate of ~1.9 Gt $CaCO_3$/yr (Wallacea only accounts for ~0.5 Gt $CaCO_3$/yr), and moderately decreased afterward. Such variations are not specific to the last glacial cycle but are representative of any (although peak productivities vary from ~0.5 Gt $CaCO_3$/yr to ~8 Gt $CaCO_3$/yr, Figure 8a). At present day, computed production rates decrease to half peak Holocene rates, in the same range as carbonate productivities derived from field observations (0.65–0.83 Gt $CaCO_3$/yr for modern rates; Milliman, 1993; Vecsei, 2004). For comparison, this value is in the same range as the current mean annual sediment discharge of major rivers like the Amazon (1.2 Gt/yr; Meade et al., 1985; Milliman & Syvitski, 1992).

Over the long term, throughout the course of the Pleistocene glaciations, reef productivity moderately varies (Figure 8a). The role of uplift and subsidence however most importantly sets reef productivity. Assuming that the probability density function of Figure 1 for uplift holds in the intertropical zone, the bulk production of reef carbonates increases threefold with respect to uplift-deprived cases. Conversely, the effect of slope distribution is negligible.

The bulk volume of sequences of fossil coral reefs is, to our knowledge, unknown. Our models provide a first order, indirect, estimate of this metric. After 1,500 kyr, our results suggests that reefs in the intertropical zone precipitated approximately $0.8 \times 10^6$ Gt $CaCO_3$. For comparison, this corresponds to the deposition of some $500 \times 10^3$ $km^3$, i.e., the equivalent of a uniform, 1 m-thick layer spread over the entire Earth, laid over 1.5 Myr; or approximately the volume of the mountains of the Alps in 1 Myr.

Our probabilistic analysis agrees with the theoretical analysis (see section 4) and suggests that the production rate slightly increased as a response to the changing pace of sea level oscillations during Mid-Pleistocene. Before the MPT, in the 40 kyr world, the mean production rate was 0.39 Gt $CaCO_3$/yr (Figure 8a); it increased by a factor 1.4 to meet a mean productivity of 0.55 Gt $CaCO_3$/yr during the MPT, and

returned to 0.40 Gt $CaCO_3$/yr in the 100 kyr world, well after the end of the MPT, at ~400 ka. The modeled increased productivity during the MPT not only relies on the higher and longer lasting production peaks during the MPT but also relies on the mean production that is slightly higher than before and after the MPT (Figure 8a). Whether such variations have an impact on the emergence of the major reef systems remains disputable on this basis, for most barrier reefs probably expanded at the end of the MPT (Cabioch et al., 2008; Montaggioni et al., 2011; Webster & Davies, 2003), and not earlier. This suggests that the emergence of these large systems is unrelated to this effect. Instead, it clearly appears that vertical ground motion much more efficiently promotes carbonate production (Figure 8a) than the changing amplitude and frequencies of the glacial cycle. In the geodynamically active intertropical zone—the Caribbean and SE Asian realms in particular—we suggest that vertical ground motion is thus a more plausible explanation to trigger the onset of the major barrier reef systems.

## 7. Discussion: Chemical Budget

Our models predict that carbonate productivity temporally varies by several orders of magnitude (Figure 8a). Because productivity waxes and wanes throughout the glacial cycle, the intake and egress of chemical elements from the oceanic and atmospheric reservoirs varies accordingly, as readily suggested by the calcification equation, that writes $Ca^{2+} + 2HCO_3^- \rightarrow CaCO_3 + CO_2 + H_2O$. More specifically, it suggests that coral reefs may modulate the calcium and carbon budgets. Different time scales shall be considered in that respect: the late Holocene (and present day), the glacial cycle (transgression and regression), and the long term (~ 1 Myr).

### 7.1. Calcium

Each precipitated mole of calcium carbonate depletes the oceans from 1 mol of $Ca^{2+}$ as well as 2 mol of $HCO_3^-$. Integrated over the intertropical zone, our model yields an estimated mean productivity of ~0.5 Gt $CaCO_3$/yr over the last 1,500 years (Figure 8a), i.e., $5\times 10^{12}$ mol/yr. These values, and their temporal evolution, shall be compared to sources and sinks of calcium. Being part of a major element system, the calcium carbonate is commonly scrutinized. Yet quantifications remain uncertain, in particular with respect to the neretic and pelagic accumulation rates (e.g., Milliman & Droxler, 1996).

At present day, the river input in calcium and carbonate is fairly well constrained and amounts to $15\times 10^{12}$ mol/yr (Holland, 2005, after Meybeck (2003)). According to Holland (2005), $CaCO_3$ input globally balances $CaCO_3$ output, with a net flux of $17.6\times 10^{12}$ mol/yr ±20%, where $15.7\times 10^{12}$ mol/yr are precipitated. Our results (~0.8 Gt $CaCO_3$/yr, or $8\times 10^{12}$ mol/yr, for the Late Holocene) would thus imply that coral reefs in the intertropical zone currently contribute by as much as 50% to the global Ca budget. However, the present-day steady state hypothesis advocated by Holland (2005) is uncertain (Milliman & Droxler, 1996), for sinks are in fact known within a very large range. Sinks at present day could amount to ~3.2 Gt $CaCO_3$/yr, or $32\times 10^{12}$ mol/yr (Milliman, 1993). Our estimates are in accord with (Milliman, 1993), who proposes that modern coral reefs contribute to neretic accumulation of calcium carbonates by ~0.7 Gt $CaCO_3$/yr (~$7\times 10^{12}$ mol/yr), i.e., 22% of the total accumulation that amounts to ~3.2 Gt $CaCO_3$/yr. This value shall be confronted to estimates of Ca and $CO_3$ inputs (fluvial, hydrothermal, and possibly groundwater), that sum up to 2.1–3.0 Gt $CaCO_3$/yr, revealing that present-day outputs overtake inputs (Milliman, 1993; Milliman & Droxler, 1996).

This imbalance is found for Late Holocene or present-day estimates, where reef productivity surpasses the mean value (Figure 8a). However, peak productivities are higher; our model predicts values as high as 1.9 Gt $CaCO_3$/yr (peak Holocene), 2.5–4.5 Gt $CaCO_3$/yr (MIS5e transgression and most late deglaciation times), and more than 10 Gt $CaCO_3$/yr at ~404 kyr (MIS11) and ~1,070 kyr (MIS 31). Assuming a maximum input of 3 Gt $CaCO_3$/yr (Milliman & Droxler, 1996) and holding all other outputs constant, oceans were depleted in calcium by reef sequestration during these periods of peak productivities by as much as 1.4, 2–4, and up to 9.5 Gt $CaCO_3$/yr, respectively. For a total oceanic mass of calcium of $5.31\times 10^{20}$ g ($1{,}370\times 10^6$ km$^3$ of oceanic water concentrated at 411 mg Ca/L), it depletes the oceanic calcium every thousand years by 1‰, 1.5–3‰, and up to 7‰ of the total mass of calcium, respectively. Peak productivities typically last for a few kyr (Figure 8a), which would therefore deplete the oceanic reservoir by a few ‰, and occasionally up to a few %, during these periods. Most critical are MIS11 and MIS31, for productivities reach higher values for longer periods of time and, following this approach, the calcium depletion could have been more severe.

Conversely, coral reefs could seriously attenuate and even reverse this disequilibrium during periods of lesser productivity. Indeed, regressions are characterized by low reef productivities, at least an order of magnitude lower than during transgressions. Depending on the uncertain contribution of groundwater $CaCO_3$ (Milliman & Droxler, 1996), periods of lowermost productivities could be marked by a recharge of the oceanic reservoir by up to 0.5 Gt $CaCO_3$/yr, provided inputs remain constant. Because these periods of time last much longer than periods of peak productivities (Figure 8a), they possibly restore the balance between inputs and outputs at longer, Plio-Quaternary time scales.

On such time scales, throughout the glacial cycle, reef productivity amounts to ~0.5 Gt $CaCO_3$/yr, almost half the modern value (Milliman, 1993; Vecsei, 2004, and current study). These results imply that coral reefs in the intertropical zone contribute by as much as 30% of the precipitated calcium carbonate (following estimates of Holland, 2005), and 11%–24% of the total input from rivers, hydrothermalism, and groundwater (following Milliman & Droxler, 1996). Despite the uncertainty in the estimated input, these results suggest that over longer time scales, steady state could hold, with alternating short periods of largely excessive calcium sequestrations during peak productivities and longer periods of calcium sequestration deficit. In that respect, coral reefs shall not be regarded as having a buffering effect on the calcium disequilibriums, but instead as having an aggressive behavior on the calcium budget, yet self-adjusted on the long term.

Last, over time scales deeper than that of the Plio-Quaternary, the modulating effect of coral reefs on the calcium carbonate budget shall be considered. Our models show that Mid to Late Quaternary glacial oscillations efficiently stimulate reef productivity. At earlier times, the profound effect that recent glacial cycles have on coral reefs could not prevail, and reef productivity was therefore much lower. If input calcium carbonate remained constant, it implies that imbalance between inputs and outputs better hold, and that only the Plio-Quaternary glaciations triggered the departure from steady state. This departure is moderate (see above) and within the range of uncertainty given by direct measurements of Ca riverine inputs (Tipper et al., 2010).

### 7.2. Carbon Dioxide

Simultaneously, the calcification equation indicates that 1 mol of $CO_2$ and 1 mol of $H_2O$ are in principle released, which is sometimes thought to substantially contributes to changes in atmospheric $pCO_2$. An end-member model is that of the *coral reef hypothesis* (Berger, 1982; Vecsei & Berger, 2004) that asserts that reef growth modifies the carbon balance and in turns, the atmospheric $pCO_2$. Although a thorough analysis of the underlying foundations of this theory is beyond the scope of the current study, we note that counterarguments oppose this theory. For instance, observed rates of benthic $CaCO_3$ deposition do not match expectations (Archer et al., 2000). Along the same lines, the expected relative timing of changes in sea level, atmospheric $CO_2$, temperature is hardly corroborated by the data (Broecker & Henderson, 1998; Foster & Rohling, 2013). In the framework of the *coral reef hypothesis*, fostered productivity during deglaciation (Figure 4) is an additional $CO_2$ source that may modulate the climate if $CO_2$ sinks do not adjust simultaneously. Because of the buffering effect of the oceans, a maximum of 0.6 mol are actually emitted for each mole of precipitated carbonate (Ware et al., 1992). Assuming a density of 2,950 kg/m$^3$ for aragonite and a bulk reef porosity of 50% (e.g., Hopley, 2011), every cubic meter of precipitated $CaCO_3$ thus matches an emission of 8,850 mol $CO_2$, i.e., 389 kg $CO_2$. It is therefore possible, in principle, to jointly quantify the reef carbonate productivity and the associated emissions of carbon dioxide. Of course, by scaling carbonate productivity to carbon dioxide emissions below, we analyze the sole intake of $CO_2$ from coral reefs and do not attempt to devise a budget. We quantify the raw fluxes, for a thorough analysis would impose to account for variations in the amounts of dissolved inorganic carbon and alkalinity, and subsequent depth variations of the lysocline (see e.g., Sigman & Boyle, 2000).

On the basis of our estimates of carbonate productivity (Figure 8a), one finds that peak productivity (~5–6 kyr prior to sea level highstands, ~10 ka in the Holocene) amounts to ~0.5 Gt $CO_2$/yr (Figure 8b). Emission rates decrease to ~0.25 Gt $CO_2$/yr at present day, which compares well to the value derived by (Ware et al., 1992) on the basis of modern reef productivity measurements and mass balance of $CaCO_3$ (Smith & Kinsey, 1976). (For comparison, this contribution nevertheless remains negligible with respect to the anthropogenic $CO_2$ emissions [37Gt $CO_2$/yr, IPCC et al., 2014].) Integrated over the deglaciation time (between 20 and 7 ka), our models predict a net emission of ~5,000 Gt $CO_2$ for the entire intertropical zone.

Atmospheric $CO_2$ is recorded in ice cores for the last 800 ka (Figure 8b, after Lüthi et al., 2008) and allows for comparison with model predictions. Predicted $CO_2$ emissions increase systematically at the end of glaciations, and peak 5 ±3 kyr before sea level highstands (see section 3.1) and often with peaks in atmospheric

$CO_2$. This indicates that variations in reef carbonate production cannot be ruled out as a potential driver of atmospheric $CO_2$ variations. During the last deglaciation, the atmospheric concentration of carbon dioxide has risen from about 180 to 270 ppmv (Lüthi et al., 2008; Petit et al., 1999).

Following the simplifications of the coral reef hypothesis, one finds from the molar budget in the atmosphere that the release of 1 $Gt\,CO_2/yr$ increases atmospheric $pCO_2$ by $\sim$0.13 ppmv. Therefore, the reef source of carbon dioxide could theoretically raise $pCO_2$ by several hundreds ppmv since the Last Glacial Maximum, which largely exceeds the observed changes in atmospheric $CO_2$ during the same period. But on a time scale of a few hundred years, only $\sim$75% of the $CO_2$ is actually dissolved in the oceans, and on the deglaciation time scale (a few thousand years, after carbonate compensation on the seabed), only $\sim$10% remain in the atmosphere Archer et al. (1997), i.e., $\sim$30 ppm. Our results are therefore compatible with the coral reef hypothesis.

## 8. Conclusions

Our innovative numerical modeling of long-term evolution of fossil coral reef sequences provides us with a theoretical approach to long-standing issues that are difficultly addressed from the geologic record. In particular, these models allow for quantitative estimates of coral reef calcium carbonate productions as well as carbon and calcium budgets. Our modeling strategy follows the same lines as a series of earlier attempts (e.g., Bosscher & Schlager, 1992; Koelling et al., 2009; Toomey et al., 2013; Turcotte & Bernthal, 1984; Warrlich et al., 2002). But here, instead of simply reproducing documented examples, we extrapolated the models to yield global quantifications of reef carbonate productivity at a global scale, with the caveat of extrapolations inherent to theoretical models. One could hope to improve such predictions with a refined integration of all processes (like including aerial erosion or opting a three-dimensional approach), but this objective simply remains beyond the current knowledge.

Many geological processes stimulate or hamper the productivity of coral reefs in a nonnegligible way, and therefore can alter geochemical equilibriums. Among those of course, sea level oscillations are a primordial control on reef production, by alternatively exposing different levels of the shore to reef construction, and therefore episodically rejuvenating the accommodation space. This implies that the onset of the glacial cycle gradually fostered reef productivity until present-day, post-MPT, sea level oscillations. Our results show that during the glacial cycle, vertical ground motion is as important as eustasy and modulates productivity by at least an order of magnitude. Of course, additional complexities to the simplified parametrization that tractable models require would modify the prediction of a given simulation. But this is beyond our goal, simply because we aim for a probabilistic approach, not for a collection of particular cases.

Considering realistic estimates of geological forcings, our results suggest that reef production responds efficiently to extrinsic processes. During the deglaciation, productivity reaches its maximum rates 4000–5000 years prior to sea level highstands, at the time of maximum transgressions, and reaches minimal values—often negligible—during sea level highstands and lowstands. During the Mid to Late Quaternary, our simulations suggest a mean productivity of $\sim$0.5 $Gt\,CaCO_3/yr$, i.e., approximately $0.75 \times 10^6$ $Gt\,CaCO_3$ over 1,500 kyr.

Implications for the chemical fluxes with the atmosphere and oceans are large. For instance, we infer that over the Mid to Late Quaternary, the calcium intake from coral reefs amounts to almost a 10–30% of the total budget. At the time scale of the glacial cycle, the associated release of carbon dioxide possibly modulates the atmospheric $pCO_2$, for reef carbonate productivity, and $CO_2$ emissions, vary coevally with sea level oscillations. Deriving definitive values is beyond our simplified approach of the chemical balance, but our results with no doubt emphasize the primordial role of coral reefs on the carbon and calcium cycles.

**Acknowledgments**
Source code is available upon request to L.H. and A-M.P., or from their professional webpages. The manuscript benefited from the useful reviews of Martin Koelling and an anonymous reviewer.

## References

Alexander, I., Andres, M., Braithwaite, C., Braga, J., Cooper, M., Davies, P., et al. (2001). New constraints on the origin of the Australian Great Barrier Reef: Results from an international project of deep coring. *Geology*, *29*, 483. https://doi.org/10.1130/0091-7613(2001)029<0483:NCOTOO>2.0.CO;2

Archer, D., Kheshgi, H., & Maier-Reimer, E. (1997). Multiple timescales for neutralization of fossil fuel $CO_2$. *Geophysical Research Letters*, *24*(4), 405–408. https://doi.org/10.1029/97GL00168

Archer, D., Winguth, A., Lea, D., & Mahowald, N. (2000). What caused the glacial/interglacial atmospheric $pCO_2$ cycles? *Reviews of Geophysics*, *38*(2), 159–189. https://doi.org/10.1029/1999RG000066

Barrett, S. J., & Webster, J. M. (2012). Holocene evolution of the Great Barrier Reef: Insights from 3D numerical modelling. *Sedimentary Geology*, *265–266*, 56–71. https://doi.org/10.1016/j.sedgeo.2012.03.015
Berger, W. H. (1982). Increase of carbon dioxide in the atmosphere during deglaciation: The coral reef hypothesis. *Naturwissenschaften*, *69*(2), 87–88. https://doi.org/10.1007/BF00441228
Bintanja, R., & van de Wal, R. S. W. (2008). North American ice-sheet dynamics and the onset of 100,000-year glacial cycles. *Nature*, *454*(7206), 869–872. https://doi.org/10.1038/nature07158
Blanchon, P., & Eisenhauer, A. (2001). Multi-stage reef development on Barbados during the Last Interglaciation. *Quaternary Science Reviews*, *20*(10), 1093–1112. https://doi.org/10.1016/S0277-3791(00)00173-6
Blanchon, P., Eisenhauer, A., Fietzke, J., & Liebetrau, V. (2009). Rapid sea-level rise and reef back-stepping at the close of the last interglacial highstand. *Nature*, *458*(7240), 881–884. https://doi.org/10.1038/nature07933
Blanchon, P., Granados-Corea, M., Abbey, E., Braga, J. C., Braithwaite, C., Kennedy, D. M., et al. (2014). Postglacial fringing-reef to barrier-reef conversion on Tahiti links Darwin's reef types. *Scientific Reports*, *4*(1), 4997 EP.
Bosscher, H., & Schlager, W. (1992). Computer simulation of reef growth. *Sedimentology*, *39*(3), 503–512. https://doi.org/10.1111/j.1365-3091.1992.tb02130.x
Braithwaite, C. J. (2016). Coral-reef records of quaternary changes in climate and sea-level. *Earth-Science Reviews*, *156*, 137–154. https://doi.org/10.1016/j.earscirev.2016.03.002
Braithwaite, C. J. R., Dalmasso, H., Gilmour, M. A., Harkness, D. D., Henderson, G. M., Kay, R. L. F., et al. (2004). The Great Barrier Reef: The chronological record from a new borehole. *Journal of Sedimentary Research*, *74*(2), 298–310. https://doi.org/10.1306/091603740298
Broecker, W. S., & Henderson, G. M. (1998). The sequence of events surrounding Termination II and their implications for the cause of glacial-interglacial $CO_2$ changes. *Paleoceanography*, *13*(4), 352–364. https://doi.org/10.1029/98PA00920
Burke, L., Reytar, K., Spalding, M., & Perry, A. (2011). *Reefs at risk* (130 pp.). Washington, DC: World Resources Institute.
Cabioch, G., Montaggioni, L., Thouveny, N., Frank, N., Sato, T., Chazottes, V., et al. (2008). The chronology and structure of the western new Caledonian Barrier Reef tracts. *Palaeogeography, Palaeoclimatology, Palaeoecology*, *268*(1–2), 91–105. https://doi.org/10.1016/j.palaeo.2008.07.014
Camoin, G. F., & Webster, J. M. (2015). Coral reef response to quaternary sea-level and environmental changes: State of the science. *Sedimentology*, *62*(2), 401–428. https://doi.org/10.1111/sed.12184
Caputo, R. (2007). Sea-level curves: Perplexities of an end-user in morphotectonic applications. *Global and Planetary Change*, *57*(3–4), 417–423. https://doi.org/10.1016/j.gloplacha.2007.03.003
Doust, H., & Sumner, H. (2007). Petroleum systems in rift basins—A collective approach in southeast Asian basins. *Petroleum Geosciences*, *13*(2), 127–144.
Dullo, W.-C. (2005). Coral growth and reef growth: A brief review. *Facies*, *51*(1–4), 33–48. https://doi.org/10.1007/s10347-005-0060-y
Evans, P. (1936). The geological evidence for recent submergence of the Assam-Malay-Australia region. *Proceedings of the National Institute of Science of India*, *2*, 145–154.
Falter, J. L., Lowe, R. J., Zhang, Z., & McCulloch, M. (2013). Physical and biological controls on the carbonate chemistry of coral reef waters: Effects of metabolism, wave forcing, sea level, and geomorphology. *PLoS ONE*, *8*(1), e53303–e53319. https://doi.org/10.1371/journal.pone.0053303
Foster, G. L., & Rohling, E. J. (2013). Relationship between sea level and climate forcing by $CO_2$ on geological timescales. *Proceedings of the National Academy of Sciences of the United States of America*, *110*(4), 1209–1214. https://doi.org/10.1073/pnas.1216073110
Hanebuth, T., Stattegger, K., & Saito, Y. (2002). The stratigraphic architecture of the central Sunda Shelf (SE Asia) recorded by shallow-seismic surveying. *Geo-Marine Letters*, *22*(2), 86–94. https://doi.org/10.1007/s00367-002-0102-1
Harris, D. L., Webster, J. M., Vila-Concejo, A., Hua, Q., Yokoyama, Y., & Reimer, P. J. (2015). Late Holocene sea-level fall and turn-off of reef flat carbonate production: Rethinking bucket fill and coral reef growth models. *Geology*, *43*(2), 175. https://doi.org/10.1130/G35977.1
Holland, H. D. (2005). Sea level, sediments and the composition of seawater. *American Journal of Science*, *305*(3), 220. https://doi.org/10.2475/ajs.305.3.220
Hopley, D. (2011). *Encyclopedia of modern coral reefs: Structure, form and process, Encyclopedia of earth sciences*. Dordrecht, the Netherlands: Springer.
IPCC, Pachauri, R., & Meyer, L. (Eds.). (2014). *Climate change 2014: Synthesis report. Contribution of Working Groups I, II and III to the fifth assessment report of the Intergovernmental Panel on Climate Change* (151 pp.). Geneva, Switzerland: IPCC.
Jorry, S. J., Droxler, A. W., & Francis, J. M. (2010). Deepwater carbonate deposition in response to re-flooding of carbonate bank and atoll-tops at glacial terminations. *Quaternary Science Reviews*, *29*(17–18), 2010–2026. https://doi.org/10.1016/j.quascirev.2010.04.016
Koelling, M., Webster, J. M., Camoin, G., Iryu, Y., Bard, E., & Seard, C. (2009). SEALEX—Internal reef chronology and virtual drill logs from a spreadsheet-based reef growth model. *Global and Planetary Change*, *66*(1–2), 149–159. https://doi.org/10.1016/j.gloplacha.2008.07.011
Lüthi, D., Le Floch, M., Bereiter, B., Blunier, T., Barnola, J.-M., Siegenthaler, U., et al. (2008). High-resolution carbon dioxide concentration record 650,000–800,000years before present. *Nature*, *453*(7193), 379–382. https://doi.org/10.1038/nature06949
Meade, R. H., Dunne, T., Richey, J. E., Santos, U. D. M., & Salati, E. (1985). Storage and remobilization of suspended sediment in the lower Amazon River of Brazil. *Science*, *228*(4698), 488–490. https://doi.org/10.1126/science.228.4698.488
Meybeck, M. (2003). Global occurrence of major elements in rivers. *Treatise on Geochemistry*, *5*, 605. https://doi.org/10.1016/B0-08-043751-6/05164-1
Milliman, J. D. (1993). Production and accumulation of calcium carbonate in the ocean: Budget of a nonsteady state. *Global Biogeochemical Cycles*, *7*(4), 927–957. https://doi.org/10.1029/93GB02524
Milliman, J. D., & Droxler, A. W. (1996). Neritic and pelagic carbonate sedimentation in the marine environment: Ignorance is not bliss. *Geologische Rundschau*, *85*(3), 496–504. https://doi.org/10.1007/BF02369004
Milliman, J. D., & Syvitski, J. P. M. (1992). Geomorphic/tectonic control of sediment discharge to the ocean: The importance of small mountainous rivers. *Journal of Geology*, *100*(5), 525–544. https://doi.org/10.1086/629606
Molnar, P., & Cronin, T. W. (2015). Growth of the maritime continent and its possible contribution to recurring ice ages. *Paleoceanography*, *30*, 196–225. https://doi.org/10.1002/2014PA002752
Montaggioni, L., & Braithwaite, C. (2009). *Quaternary coral reef systems: History, development processes and controlling factors, developments in marine geology*. Amsterdam, the Netherlands: Elsevier.
Montaggioni, L. F. (2005). History of Indo-Pacific coral reef systems since the last glaciation: Development patterns and controlling factors. *Earth Science Reviews*, *71*(1–2), 1–75. https://doi.org/10.1016/j.earscirev.2005.01.002
Montaggioni, L. F., Borgomano, J., Fournier, F., & Granjeon, D. (2015). Quaternary atoll development: New insights from the two-dimensional stratigraphic forward modelling of Mururoa Island (central Pacific Ocean). *Sedimentology*, *62*(2), 466–500. https://doi.org/10.1111/sed.12175

Montaggioni, L. F., Cabioch, G., Thouveny, N., Frank, N., Sato, T., & Sémah, A.-M. (2011). Revisiting the quaternary development history of the western new Caledonian Shelf System: From ramp to barrier reef. *Marine Geology*, *280*(1–4), 57–75. https://doi.org/10.1016/j.margeo.2010.12.001

Multer, H. G., Gischler, E., Lundberg, J., Simmons, K. R., & Shinn, E. A. (2002). Key largo limestone revisited: Pleistocene shelf-edge facies, Florida Keys, USA. *Facies*, *46*(1), 229–271. https://doi.org/10.1007/BF02668083

Murray-Wallace, C., & Woodroffe, C. (2014). *Quaternary sea-level changes*. Cambridge, UK: Cambridge University Press.

Neumann, A. C., & Macintyre, I. (1985). *Reef response to sea-level rise: Keep-up, catch-up or give-up*. Paper presented at the Proceedings of the Fifth International Coral Reef Congress (Vol. 2, pp. 105–110).

Opdyke, B. N., & Walker, J. C. G. (1992). Return of the coral reef hypothesis: Basin to shelf partitioning of $CaCO_3$ and its effect on atmospheric $CO_2$. *Geology*, *20*(8), 733. https://doi.org/10.1130/0091-7613(1992)020<0733:ROTCRH>2.3.CO;2

Past Interglacials Working Group of PAGES. (2016). Interglacials of the last 800,000 years. *Reviews of Geophysics*, *54*, 162–219. https://doi.org/10.1002/2015RG000482

Pedoja, K., Husson, L., Johnson, M. E., Melnick, D., Witt, C., Pochat, S., et al. (2014). Coastal staircase sequences reflecting sea-level oscillations and tectonic uplift during the Quaternary and Neogene. *Earth Science Reviews*, *132*, 13–38. https://doi.org/10.1016/j.earscirev.2014.01.007

Pedoja, K., Husson, L., Regard, V., Cobbold, P. R., Ostanciaux, E., Johnson, M. E., et al. (2011). Relative sea-level fall since the last interglacial stage: Are coasts uplifting worldwide? *Earth Science Reviews*, *108*(1–2), 1–15. https://doi.org/10.1016/j.earscirev.2011.05.002

Petit, J. R., Jouzel, J., Raynaud, D., Barkov, N. I., Barnola, J.-M., Basile, I., et al. (1999). Climate and atmospheric history of the past 420,000 years from the Vostok ice core, Antarctica. *Nature*, *399*(6735), 429–436. https://doi.org/10.1038/20859

Pirazzoli, P. A., Radtke, U., Hantoro, W. S., Jouannic, C., Hoang, C. T., Causse, C., et al. (1991). Quaternary raised coral-reef terraces on Sumba island, Indonesia. *Science*, *252*(5014), 1834–1836. https://doi.org/10.1126/science.252.5014.1834

Scoffin, T. P., & Tissier, M. D. A. L. (1998). Late Holocene sea level and reef-flat progradation, Phuket, South Thailand. *Coral Reefs*, *17*(3), 273–276. https://doi.org/10.1007/s003380050128

Sigman, D. M., & Boyle, E. A. (2000). Glacial/interglacial variations in atmospheric carbon dioxide. *Nature*, *407*, 859–869. https://doi.org/10.1038/35038000

Smith, S. V., & Kinsey, D. W. (1976). Calcium carbonate production, coral reef growth, and sea level change. *Science*, *194*(4268), 937–939. https://doi.org/10.1126/science.194.4268.937

Speed, R. C., & Cheng, H. (2004). Evolution of marine terraces and sea level in the last interglacial, Cave Hill, Barbados. *Geological Society of America Bulletin*, *116*(1), 219. https://doi.org/10.1130/B25167.1

Tipper, E., Gaillardet, J., Galy, A., Louvat, P., Bickle, M., & Capmas, F. (2010). Calcium isotope ratios in the world's largest rivers: A constraint on the maximum imbalance of oceanic calcium fluxes. *Global Biogeochemical Cycles*, *24*, GB3019. https://doi.org/10.1029/2009GB003574

Tomascik, T. (1997). *The ecology of the Indonesian Seas: Chapters 13–23, The ecology of the Indonesian Seas*. Jakarta, Indonesia: Periplus Editions.

Toomey, M., Ashton, A. D., & Perron, J. T. (2013). Profiles of ocean island coral reefs controlled by sea-level history and carbonate accumulation rates. *Geology*, *41*(7), 731–734. https://doi.org/10.1130/G34109.1

Turcotte, D. L., & Bernthal, M. J. (1984). Synthetic coral-reef terraces and variations of Quaternary sea level. *Earth and Planetary Science Letters*, *70*(1), 121–128. https://doi.org/10.1016/0012-821X(84)90215-2

Vecsei, A. (2004). A new estimate of global reefal carbonate production including the fore-reefs. *Global and Planetary Change*, *43*(1–2), 1–18. https://doi.org/10.1016/j.gloplacha.2003.12.002

Vecsei, A., & Berger, W. H. (2004). Increase of atmospheric $CO_2$ during deglaciation: Constraints on the coral reef hypothesis from patterns of deposition. *Global Biogeochemical Cycles*, *18*, GB1035. https://doi.org/10.1029/2003GB002147

Verbeek, R. (1908). *Rapport sur les Moluques: Reconnaissances géologiques dans la partie orientale de l'Archipel des Indes Orientales Néerlandaises*. Batavia, Indonesia: Imprimerie de l'Etat.

Ware, J. R., Smith, S. V., & Reaka-Kudla, M. L. (1992). Coral reefs: Sources or sinks of atmospheric $CO_2$? *Coral Reefs*, *11*(3), 127–130. https://doi.org/10.1007/BF00255465

Warrlich, G. M. D., Waltham, D. A., & Bosence, D. W. J. (2002). Quantifying the sequence stratigraphy and drowning mechanisms of atolls using a new 3-D forward stratigraphic modelling program (carbonate 3D). *Basin Research*, *14*(3), 379–400. https://doi.org/10.1046/j.1365-2117.2002.00181.x

Webster, J. M., & Davies, P. J. (2003). Coral variation in two deep drill cores: Significance for the Pleistocene development of the Great Barrier Reef. *Sedimentary Geology*, *159*(1–2), 61–80. https://doi.org/10.1016/S0037-0738(03)00095-2

Wilson, M. E. J. (2011). SE Asian carbonates: Tools for evaluating environmental and climatic change in equatorial tropics over the last 50 million years. *Geological Society, Special Publications*, *355*(1), 347–372. https://doi.org/10.1144/SP355.18

Wong, H., Ludmann, T., Haft, C., Paulsen, A.-M., Hubscher, C., & Geng, J. (2003). Quaternary sedimentation in the Molengraa!' paleo-delta, northern Sunda Shelf (southern South China Sea). In F. Sidi et al. (Eds.), *Tropical deltas of Southeast Asia—Sedimentology, stratigraphy, and petroleum geology* (pp. 20–216).

Woodroffe, C. D., & Webster, J. M. (2014). Coral reefs and sea-level change. *Marine Geology*, *352*, 248–267. https://doi.org/10.1016/j.margeo.2013.12.006

Yamamoto, K., Iryu, Y., Sato, T., Chiyonobu, S., Sagae, K., & Abe, E. (2006). Responses of coral reefs to increased amplitude of sea-level changes at the Mid-Pleistocene climate transition. *Palaeogeography, Palaeoclimatology, Palaeoecology*, *241*(1), 160–175. https://doi.org/10.1016/j.palaeo.2006.06.014